Heliyon 5 (2019) e01863

Contents lists available at ScienceDirect

Heliyon

journal homepage: www.heliyon.com

Entropy generation and activation energy mechanism in nonlinear radiative flow of Sisko nanofluid: rotating disk

M. Ijaz [a,*], M. Ayub [a], H. Khan [b]

[a] Department of Mathematics, Quaid-I-Azam University 45320, Islamabad, 44000, Pakistan
[b] Machine Intelligence Research Labs (MIR Labs), Auburn, USA

ARTICLE INFO

Keywords:
Entropy generation
Activation energy
Non-linear thermal radiation
Sisko nano-fluid model
Non-uniform heat source/sink
Non-linear mixed convection
Rotating stretchable disk
Thermodynamics
Mechanics
Mechanical engineering

ABSTRACT

The theme of the present communication is to explore the novel analysis of entropy generation optimization, binary chemical reaction and activation energy for nonlinear convective flow of Sisko model on a radially stretchable rotating disk in the presence of a uniform vertical magnetic field. Nonlinear mixed convection, nonlinear thermal radiation, MHD, viscous dissipation, Joule heating and non-uniform heat generation/absorption are also considered. Nanofluid model includes significant slip mechanism of Brownian motion and thermophoresis. Apposite transformations are endorsed to get the nonlinear coupled ODEs system. The resultant system of ordinary differential equations is endeavoured for series solutions through homotopic technique. Total entropy generation is inspected through numerous emerging flow variables. Comparative study is made for temperature, velocity, heat transfer rate, Bejan number, entropy generation and mass transfer Nusselt number by considering shear thickening and thinning fluids. Finally, a comparison is specified with the previous existing results.

1. Introduction

Fluid flow over rotating surfaces has been analysed extensively in view of its engineering and industrial applications. The fluid flow due to rotating surfaces is used in electric-power generating system, air cleaning machine, medical equipment, gas turbines, turbine system, food processing technology and aero-dynamical engineering [1, 2, 3]. Therefore experimental and theoretical work related to this type of flow appears to be very fascinating. Firstly, Karman [4] has introduced significant similarity transformations for the fluid flow problem over a disk. Heat and mass transfer analysis of viscous fluid through a porous rotating disk is numerically investigated by Turkyilmazoglu [5]. Mair et al. [6] discussed the diffusion and slip mechanism for Carreau–Yasuda fluid over a rotating disk. Heat transfer of hydro-magnetic Couette flow in a rotating system with variable viscosity and Hall effects is considered by Makinde et al. [7]. Radiative flow problem due to a stretchable rotating disk in presence of variable thickness is measured by Hayat et al. [8] through homotopic technique. Babu and Sandeep [9] investigated thermophoresis and Brownian motion effects for 3-dimensional flow of nanofluids with MHD and slip effects. Hayat et al. [10] explored the slip mechanism by a variable thickness rotating disk subject to MHD. The study of entropy generation on hydro-magnetic nanoliquid flow over a porous rotating disk was thought out by Rashidi et al. [11]. Hayat et al. [12] exposed the impact of MHD flow of Cu–H_2O based nanoliquid due to a rotating disk with slip mechanism. Hayat et al. [13] deliberated the combined influences of thermal radiation and heat generation/absorption on Maxwell nanofluid over a stretched surface. A numerical analysis has been executed by Raju et al. [14] for Cu-kerosene nanoliquid with MHD over a cone surface.

The consequence of thermal radiation on MHD flow and heat transfer problem is gradually becoming important in many industries. Heat transfer by thermal radiation has enormous applications in different technological processes such as nuclear power plants, satellites and space vehicles, gas turbines and the numerous propulsion devices for aircraft. The linear radiation based on linearized Rosseland approximation is not critically effective/valid for high temperature differences. Since linearized Rosseland approximation depends upon unique Prandtl number [15], whereas in the nonlinear Rosseland approximation, the problem is governed by three main factors, known as radiation parameter, Prandtl number and the temperature ratio parameter. Primarily, Pantokratoras [16] considered the impact of Rosseland radiation for linear and nonlinear phenomena on natural convection along a vertical isothermal plate using another radiation factor stated as film radiation parameter. Khan et al. [17] discussed thermal diffusion stagnation point Maxwell

* Corresponding author.
E-mail address: misbahijaz@math.qau.edu.pk (M. Ijaz).

https://doi.org/10.1016/j.heliyon.2019.e01863
Received 12 September 2018; Received in revised form 28 January 2019; Accepted 12 May 2019

nanofluid flow with solar radiation and thermal conductivity. Heat transfer analysis through nonlinear Rosseland approximation in presence of MHD over a stretched sheet is observed by Mushtaq et al. [18]. Ijaz and Ayub [19] presented radiative flow of ferromagnetic Maxwell fluid in presence of dual stratification and magnetic dipole. Parida et al. [20] reflected the radiative flow of heat transfer over a flat surface with thermophoresis and slip mechanism. Cortell [21] performed numerical investigated for the flow problem of quiescent fluid in view of nonlinear Rosseland thermal radiation over a stretched sheet. Some significant investigations related to the topic can be viewed via Refs. [22, 23, 24, 25].

The multi-complex rheology of biological fluids has stimulated investigations including numerous non-Newtonian liquids. In recent years, studies of non-Newtonian liquids have gained extra significance due to their connection in mechanical and industrial applications. Mainly such fluids are experienced in the synthetic and automatic processes, material handling, businesses, oil store building foods stuffs and many others. Stress tensor in such material is associated to the shear rate by non-linear relation. The Sisko [26] fluid model predicts the rheology of both dilatant and pseudoplastic fluids based on the significant range of shear rates. This model can be acknowledged as more generalized version of power law liquids. It includes both power law and viscous models. Hayat et al. [27] elaborated the effects of mass suction/injection for unsteady, incompressible Sisko liquid over a stretched surface. Malik et al. [28] has investigated the magneto-hydrodynamic flow of Sisko fluid and heat transmission with convective boundary condition over a nonlinearly stretching sheet. Convective flow of Sisko model over a bidirectional stretched sheet is presented by Munir et al. [29]. Convective heat transfer and variable thermal conductivity of Sisko nanofluid towards a stretched cylinder is discussed by Khan et al. [30].

The main theme of the present communication is to examine irreversibility of nonlinear convective flow of Sisko nanofluid over a stretched rotating disk in the presence of binary chemical reaction and activation energy. The originality of problem is to discover the entropy generation optimization for Sisko model with significant features of non-uniform heat source/sink, binary chemical reaction, nonlinear thermal radiation, nonlinear mixed convection, and activation energy. Sisko nanomaterial model is used which defines the important slip mechanism namely Brownian and thermophoresis diffusions. Total entropy generation rate of system is estimated through several flow variables. Convergent solutions of highly nonlinear problem are obtained by using homotopy analysis method [31, 32, 33, 34, 35, 36, 37, 38, 39]. Homotopy analysis method (HAM) is one of the best efficient methods in solving different type of nonlinear differential equations such as coupled, decoupled, homogeneous and non-homogeneous. Entropy generation rate, Bejan number, Nusselt, Sherwood numbers and fluid flow features are discussed in detail through graphs and tables.

1.1. Model

Consider the incompressible boundary layer nonlinear convective flow of Sisko nanofluid with detail analysis of entropy generation and Bejan numbers due to rotating stretchable disk having angular velocity Ω_a around z-axis. Effects of nonlinear thermal radiation, binary chemical reaction, activation energy, Joule heating, nonlinear mixed convection and non-uniform heat generation/absorption are accounted in the present flow problem. The velocity components (u_1, v_1, w_1) are adopted in the direction of increasing (r_1, ϕ_1, z_1). The flow configuration of the system is presented in Fig. 1. It is also assumed that a uniform magnetic field of intensity (B_1) acts in the z-direction. Magnetic Reynolds number is considered to be small so that the induced magnetic field is negligible in comparison with the applied magnetic field. Flow is generated due to linear stretching of disk in radial direction with stretching rate S_1. The governing laws of mass, momentum, energy and concentrations [40, 41] for the present flow situation are presented in Eqs. (1), (2), (3), (4), and (5).

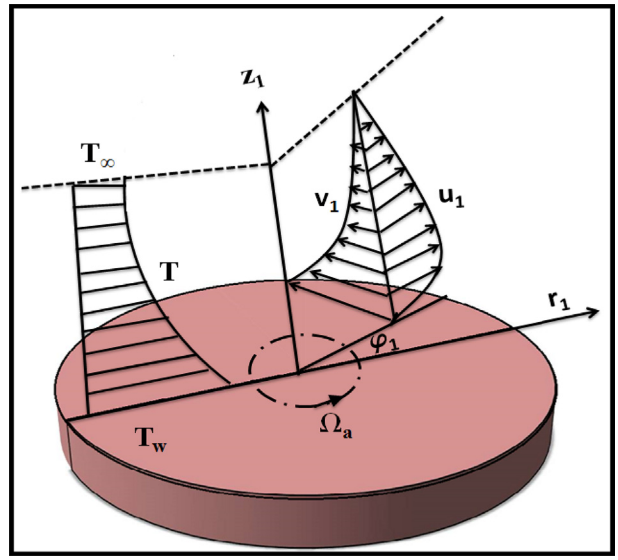

Fig. 1. Physical model.

$$\frac{\partial u_1}{\partial r_1}+\frac{u_1}{r_1}+\frac{\partial w_1}{\partial z_1}=0, \tag{1}$$

$$\left.\begin{aligned} &u_1\frac{\partial u_1}{\partial r_1}+w_1\frac{\partial u_1}{\partial z_1}-\frac{v_1^2}{r_1}=\frac{\alpha_1}{\rho_f}\frac{\partial^2 u_1}{\partial z_1^2}+\frac{\beta_1}{\rho_f}\frac{\partial}{\partial z_1}\left(\frac{\partial u_1}{\partial z_1}\left(\left(\frac{\partial u_1}{\partial z_1}\right)^2+\left(\frac{\partial v_1}{\partial z_1}\right)^2\right)^{(n-1)/2}\right)\\ &+\frac{\widehat{g}_1}{\rho_f}\left[\Xi_1(T-T_\infty)+\Xi_2(T-T_\infty)^2+\Xi_3(C-C_\infty)+\Xi_4(C-C_\infty)^2\right]-\frac{\sigma_2 B_1^2 u_1}{\rho_f},\end{aligned}\right\} \tag{2}$$

$$\left.\begin{aligned} &u_1\frac{\partial v_1}{\partial r_1}+w_1\frac{\partial v_1}{\partial z_1}-\frac{u_1 v_1}{r_1}=\frac{\alpha_1}{\rho_f}\frac{\partial^2 v_1}{\partial z_1^2}-\frac{\sigma_f B_1^2 u_1}{\rho_f}\\ &+\frac{\beta_1}{\rho_f}\frac{\partial}{\partial z_1}\left(\frac{\partial v_1}{\partial z_1}\left(\left(\frac{\partial u_1}{\partial z_1}\right)^2+\left(\frac{\partial v_1}{\partial z_1}\right)^2\right)^{(n-1)/2}\right),\end{aligned}\right\} \tag{3}$$

$$\left.\begin{aligned} &u_1\frac{\partial T}{\partial r_1}+w_1\frac{\partial T}{\partial z_1}=\frac{\widehat{\alpha}_f}{\rho_f}\frac{\partial^2 T}{\partial z_1^2}+\check{\tau}_1\widehat{D}_B\left(\frac{\partial C}{\partial r_1}\frac{\partial T}{\partial r_1}\right)+\frac{\tau_1\widehat{D}_T}{T_\infty}\left(\frac{\partial T}{\partial r_1}\right)^2\\ &+\frac{q_m}{(\rho c_p)_f}+\frac{1}{(\rho c_p)_f}\frac{\partial}{\partial z_1}\left(\frac{16\sigma_1^* T_\infty^3}{3k_1^*}\frac{\partial T}{\partial z_1}\right)+\frac{\sigma_2 B_1^2}{(\rho c_p)_f}(u_1^2+v_1^2)+\\ &\frac{\alpha_1}{(\rho c_p)_f}\left[\left(\frac{\partial u_1}{\partial z_1}\right)^2+\left(\frac{\partial v_1}{\partial z_1}\right)^2\right]+\frac{\beta_1}{(\rho c_p)_f}\left[\left(\frac{\partial u_1}{\partial z_1}\right)^2+\left(\frac{\partial v_1}{\partial z_1}\right)^2\right]^{\frac{n+1}{2}},\end{aligned}\right\} \tag{4}$$

$$\left.\begin{aligned} &u_1\frac{\partial C}{\partial r_1}+w_1\frac{\partial C}{\partial z_1}=\widehat{D}_B\frac{\partial^2 C}{\partial z_1^2}+\frac{\widehat{D}_T}{T_\infty}\frac{\partial^2 T}{\partial z_1^2}-k_1^*(C-C_\infty)\\ &-\widehat{K}_R^2(C-C_\infty)\left(\frac{T}{T_\infty}\right)^s exp\left[-\frac{E_A}{T\widehat{k}_i}\right],\end{aligned}\right\} \tag{5}$$

Apposite boundary conditions (Eq. (6)) are

$$\left.\begin{aligned} &u_1=S_1 r_1,\quad v_1=\Omega_a r_1,\quad T=T_w,\quad C=C_w\quad at\ z_1=0,\\ &u_1\to 0,\quad v_1\to 0,\quad T\to T_\infty,\quad C\to C_\infty\quad when\ z_1\to\infty.\end{aligned}\right\} \tag{6}$$

The non-uniform heat source/sink [42] is formulated by Eq. (7)

$$q''' = \frac{U_w(z)\check{K}}{\nu r_1}\left[\widehat{B}_1(T_w-T_\infty)\frac{d\widehat{F}}{d\Psi}+\widehat{B}_2(T-T_\infty)\right], \tag{7}$$

Where $\widehat{B}_1$ and $\widehat{B}_2$ delineates the coefficients of space and temperature dependent heat generation/absorption, respectively. The absolute values of $\widehat{B}_1$ and $\widehat{B}_2$ signify internal heat generation, while non-positive values characterize the internal heat absorption. Here (Ξ_1, Ξ_2) and (Ξ_3, Ξ_4) portray for coefficient of thermal and solutal expansion parameters for linear and nonlinear form respectively, ρ_f for fluid density, T for fluid temperature, c_p for specific heat, α_f for thermal diffusivity, σ_2 defines for electrical conductivity, $(\widehat{D}_B, \widehat{D}_T)$ for Brownian and thermophoretic diffusion coefficients, α_1 stands for high shear rate viscosity, β_1 for consistency index respectively. The expression $\left(\widehat{K}_R^2\left(\frac{T}{T_\infty}\right)^s \exp\left[-\frac{E_A}{T\widehat{k}_i}\right]\right)$ is the modified Arrhenius function with $(\widehat{k}_i = 8.61 \times 10^{-5}\mathrm{eV/K})$ as Boltzmann constant, $\widehat{K}_R^2$ for chemical reaction rate constant and $S\ \varepsilon\ (-1, 1)$ for fitted rate constant, respectively.

Suitable transformations (Eq. (8)) for present flow problem are [43].

$$\left.\begin{array}{l} \Psi = z_1\left(\dfrac{\rho\Omega_a^{2-n}}{\beta_1}\right)^{\frac{1}{n+1}} r_1^{\frac{1-n}{1+n}},\quad u_1 = r_1\Omega_a\widehat{F}(\Psi) \\ v_1 = r_1\Omega_a\widehat{G}(\Psi),\quad w_1 = \left(\dfrac{\rho\Omega_a^{1-2n}}{\beta_1}\right)^{-\frac{1}{n+1}} r_1^{\frac{n-1}{n+1}}\widehat{H}(\Psi) \\ \Theta(\Psi) = \dfrac{T - T_\infty}{T_w - T_\infty},\quad \phi(\Psi) = \dfrac{C - C_\infty}{C_w - C_\infty}. \end{array}\right\} \tag{8}$$

The governing flow expressions under above transformations take the following form as mentioned in Eqs. (9), (10), (11), (12), and (13)

$$\frac{d\widehat{H}}{d\Psi} = -2\widehat{F} - \left(\frac{1-n}{1+n}\right)\Psi\frac{d\widehat{F}}{d\Psi}, \tag{9}$$

$$\left.\begin{array}{l} B_s\dfrac{d^2\widehat{F}}{d\Psi^2} + \dfrac{d}{d\Psi}\left(\dfrac{d\widehat{F}}{d\Psi}\left(\left(\dfrac{d\widehat{F}}{d\Psi}\right)^2 + \left(\dfrac{d\widehat{G}}{d\Psi}\right)^2\right)^{\frac{n-1}{2}}\right) - \left(\Psi\left(\dfrac{1-n}{1+n}\right)\widehat{F} + \widehat{H}\right)\dfrac{d\widehat{F}}{d\Psi} \\ -\widehat{F}^2 - \widehat{G}^2 + \xi_1\left[(1+\beta_t\Theta)\Theta + \widehat{N}_1(1+\beta_c\phi)\phi\right] - M_1\widehat{F} = 0, \end{array}\right\} \tag{10}$$

$$\left.\begin{array}{l} B_s\dfrac{d^2\widehat{G}}{d\Psi^2} + \dfrac{d}{d\Psi}\left(\dfrac{d\widehat{G}}{d\Psi}\left(\left(\dfrac{d\widehat{F}}{d\Psi}\right)^2 + \left(\dfrac{d\widehat{G}}{d\Psi}\right)^2\right)^{\frac{n-1}{2}}\right) - 2\widehat{F}\widehat{G} \\ -\left(\Psi\left(\dfrac{1-n}{1+n}\right)\widehat{F} + \widehat{H}\right)\dfrac{d\widehat{G}}{d\Psi} - M_1\widehat{G} = 0, \end{array}\right\} \tag{11}$$

$$\left.\begin{array}{l} \dfrac{d^2\phi}{d\Psi^2} + \left(\dfrac{\widehat{N}_t}{\widehat{N}_b}\right)\dfrac{d^2\Theta}{d\Psi^2} - PrLe\left(\Psi\left(\dfrac{1-n}{1+n}\right)\widehat{F} + \widehat{H}\right)\dfrac{d\phi}{d\Psi} - \xi_2 Sc\phi \\ -Sc\xi_3\phi(1+\delta_1\Theta)^m \exp\left[-\dfrac{\widehat{E}_a}{(1+\delta_1\Theta)}\right] = 0, \end{array}\right\} \tag{13}$$

The transformed end conditions (Eq. (14)) are

$$\left.\begin{array}{lll} \widehat{F}(0) = D_1, & \widehat{G}(0) = 1 & \widehat{H}(0) = 0, \\ \Theta(0) = 1, & \phi(0) = 1, & \lim\limits_{\Psi\to\infty}\widehat{F}(\Psi) = 0, \\ \lim\limits_{\Psi\to\infty}\widehat{G}(\Psi) = 0, & \lim\limits_{\Psi\to\infty}\Theta(\Psi) = 0, & \lim\limits_{\Psi\to\infty}\phi(\Psi) = 0. \end{array}\right\} \tag{14}$$

In the above expressions, $B_s\left(=\frac{\alpha_1}{\rho_f\Omega_a}\left(\frac{\rho_f\Omega_a^{2-n}}{\beta_1}\right)^{\frac{2}{n+1}} r_1^{2\left(\frac{1-n}{1+n}\right)}\right)$ identifies for material parameter, $M_1\left(=\frac{\sigma_2 B_1^2}{\rho_f\Omega_a}\right)$ symbolize for magnetic field parameter, $\xi_1\left(=\frac{\widehat{g}_1\Xi_1(T_w-T_\infty)}{\Omega_a^2 r_1}\right)$ for mixed convective parameter, $D_1\left(=\frac{S_1}{\Omega_a}\right)$ for stretching parameter, $\widehat{N}_1\left(=\frac{\Xi_3(C_w-C_\infty)}{\Xi_1(T_w-T_\infty)}\right)$ for ratio of concentration to thermal buoyancy forces, $\beta_t\left(=\frac{\Xi_2(T_w-T_\infty)}{\Xi_1}\right)$ for nonlinear thermal convection parameter, $Pr\left(=\frac{\Omega_a}{\alpha_f}\left(\frac{\rho_f\Omega_a^{2-n}}{\beta_1}\right)^{-\frac{2}{n+1}} r_1^{-2\left(\frac{1-n}{1+n}\right)}\right)$ for Prandtl number, $\beta_c\left(=\frac{\Xi_4(C_w-C_\infty)}{\Xi_3}\right)$ for nonlinear solutal mixed convection parameter, $Sc\left(=\frac{r_1 U_w}{\widehat{D}_B}\right)$ for Schmidt number, $Le\left(=\frac{\widehat{\alpha}_f}{\widehat{D}_B}\right)$ for Lewis number, $\left((\widehat{N}_b, \widehat{N}_t) = \left(\frac{\widehat{\tau}_1\widehat{D}_B(C_w-C_\infty)}{\alpha_f}, \frac{\widehat{\tau}_1\widehat{D}_T(T_w-T_\infty)}{T_\infty\alpha_f}\right)\right)$ for Brownian and thermophoresis parameters, $\widehat{N}_R\left(=\frac{16\sigma_1^* T_\infty^3}{3Kk_1^*}\right)$ for radiation parameter, $\xi_3\left(=\frac{\widehat{K}_R^2}{S_1}\right)$ for reaction rate constant, $\widehat{E}_a\left(=\frac{E_a}{T_\infty\widehat{k}_i}\right)$ for activation energy, $\delta_1\left(=\frac{(T_w-T_\infty)}{T_\infty}\right)$ for temperature difference and $\xi_2\left(=\frac{k_1^*}{S_1}\right)$ for chemical reaction parameter, respectively.

1.2. Entropy generation modeling

Entropy generation [44, 45, 46] for Sisko nano-model over a stretchable rotating disk is mentioned in Eq. (16)

$$\left.\begin{array}{l} \dfrac{d^2\Theta}{d\Psi^2} + \widehat{N}_b\dfrac{d\Theta}{d\Psi}\dfrac{d\phi}{d\Psi} + \widehat{N}_t\left(\dfrac{d\Theta}{d\Psi}\right)^2 + Pr\left(\widehat{B}_1\dfrac{d\widehat{F}}{d\Psi} + \widehat{B}_2\Theta\right) - Pr\left(\Psi\left(\dfrac{1-n}{1+n}\right)\widehat{F} + \widehat{H}\right)\dfrac{d\Theta}{d\Psi} \\ +\widehat{N}_R\left(3(\Theta_w - 1)\left(\dfrac{d\Theta}{d\Psi}\right)^2 + (1 + (\Theta_w - 1)\Theta)\dfrac{d^2\Theta}{d\Psi^2}\right)(1 + (\Theta_w - 1)\Theta)^2 + M_1 Ec\widehat{F}^2 \\ +M_1 Ec\widehat{G}^2 + B_s Ec\left(\left(\dfrac{d\widehat{F}}{d\Psi}\right)^2 + \left(\dfrac{d\widehat{G}}{d\Psi}\right)^2\right)^2 + Ec\left(\left(\dfrac{d\widehat{F}}{d\Psi}\right)^2 + \left(\dfrac{d\widehat{G}}{d\Psi}\right)^2\right)^{\frac{n+1}{2}} = 0, \end{array}\right\} \tag{12}$$

$$\left.\begin{aligned}&\widehat{S}_G=\frac{K}{T_\infty^2}\left[1+\frac{16\sigma_1^*T_\infty^3}{3Kk_1^*}\right]\left(\frac{\partial T}{\partial z_1}\right)^2+\frac{\widehat{D}_B}{T_\infty}\left(\frac{\partial C}{\partial z_1}\frac{\partial T}{\partial z_1}\right)+\frac{\widehat{D}_B}{C_\infty}\left(\frac{\partial C}{\partial z_1}\right)^2\\&+\frac{\mu}{T_\infty}\Phi_1+\frac{\sigma_2B_1^2}{T_\infty}\left(u_1^2+v_1^2\right).\end{aligned}\right\} \tag{15}$$

Where expression for Φ_1 is presented in (Eq. (16))

$$\Phi_1=\alpha_1\left(\left(\frac{\partial u_1}{\partial z_1}\right)^2+\left(\frac{\partial v_1}{\partial z_1}\right)^2\right)+\beta_1\left(\left(\frac{\partial u_1}{\partial z_1}\right)^2+\left(\frac{\partial v_1}{\partial z_1}\right)^2\right)^{(n+1)/2}, \tag{16}$$

We get Eq. (17) by substituting Eq. (16) into Eq. (15).

$$\left.\begin{aligned}&\widehat{S}_G=\frac{K}{T_\infty^2}\left[1+\frac{16\sigma_1^*T_\infty^3}{3Kk_1^*}\right]\left(\frac{\partial T}{\partial z_1}\right)^2+\frac{\sigma_2B_1^2}{T_\infty}\left(u_1^2+v_1^2\right)+\\&\frac{1}{T_\infty}\left[\alpha_1\left(\left(\frac{\partial u_1}{\partial z_1}\right)^2+\left(\frac{\partial v_1}{\partial z_1}\right)^2\right)+\beta_1\left(\left(\frac{\partial u_1}{\partial z_1}\right)^2+\left(\frac{\partial v_1}{\partial z_1}\right)^2\right)^{\frac{n+1}{2}}\right]\\&+\frac{\widehat{R}^*D}{T_\infty}\left(\frac{\partial C}{\partial z_1}\frac{\partial T}{\partial z_1}\right)+\frac{\widehat{R}^*D}{C_\infty}\left(\frac{\partial C}{\partial z_1}\right)^2.\end{aligned}\right\} \tag{17}$$

Eq. (18) presents four factors: (I) thermal irreversibility, (II) Joule heating irreversibility, (III) viscous dissipation on entropy generation in Sisko liquid flow and (IV) concentration irreversibility.

Entropy generation rate (Eq. (18)) in dimensionless form is

$$\left.\begin{aligned}&\widehat{N}_G=\delta_1\left(1+\widehat{N}_R\right)\left(\Theta(\Theta_w-1)+1\right)^3\Theta'^2+\widehat{B}r\left(\widehat{F}'^2+\widehat{G}'^2\right)+\frac{\widehat{B}r}{B_s}\left(\widehat{F}'^2+\widehat{G}'^2\right)^{(n+1)/2}\\&+\frac{\widehat{B}rM_1}{B_s}\left(\widehat{F}'^2+\widehat{G}'^2\right)+L^*\frac{\delta_2}{\delta_1}\phi'^2+L^*\phi'\Theta',\end{aligned}\right\} \tag{18}$$

Non-dimensional parameters are presented in Eq. (19)

$$\left.\begin{aligned}&\widehat{B}r=\frac{\alpha_1r_1^2\Omega_a^2}{K(T_w-T_\infty)},\quad \delta_1=\frac{(T_w-T_\infty)}{T_\infty},\quad \delta_2=\frac{(C_w-C_\infty)}{C_\infty},\\&\widehat{N}_G=\frac{T_\infty\widehat{S}_G}{K(T_w-T_\infty)\Omega_a}\left(\frac{\rho_f\Omega_a^{2-n}}{\beta_1}\right)^{-\frac{2}{n+1}}r_1^{-2\left(\frac{1-n}{1+n}\right)},\end{aligned}\right\} \tag{19}$$

Where $(\widehat{B}r)$, (δ_1), (δ_2) and $(\widehat{N}_G)$ defines Brinkman number, temperature difference parameter, concentration difference variable and entropy generation rate respectively.

Bejan number (Eq. (20)) in non-dimensional form is

$$\widehat{B}e=\frac{\delta_1\left(1+\widehat{N}_R\right)\left(\Theta(\Theta_w-1)+1\right)^3\Theta'^2+L^*\left(\phi'\Theta'+\frac{\delta_2}{\delta_1}\phi'^2\right)}{\left[\begin{aligned}&\delta_1\left(1+\widehat{N}_R\right)\left(\Theta(\Theta_w-1)+1\right)^3\Theta'^2+\widehat{B}r\left(1+\frac{M_1}{B_s}\right)\left(\widehat{F}'^2+\widehat{G}'^2\right)\\&+\frac{\widehat{B}r}{B_s}\left(\widehat{F}'^2+\widehat{G}'^2\right)^{(n+1)/2}+L^*\left(\phi'\Theta'+\frac{\delta_2}{\delta_1}\phi'^2\right)\end{aligned}\right]}. \tag{20}$$

Skin friction coefficient $(C_{\widehat{F}})$, local Nusselt $(Nu_{\widehat{z}})$ and Sherwood $(Sh_{\widehat{z}})$ numbers are presented in Eq. (21).

$$\left.\begin{aligned}&\frac{1}{2}C_{\widehat{F}}\left(Re_{\beta_1}\right)^{1/(n+1)}=B_s\widehat{F}''(0)-\left(-\widehat{F}''(0)\right)^n,\\&Nu_{\widehat{z}}\left(Re_{\beta_1}\right)^{-\frac{1}{n+1}}=-\left(1+(\Theta_w-1)\Theta(0)\right)^3\Theta'(0),\\&Sh_{\widehat{z}}\left(Re_{\beta_1}\right)^{-\frac{1}{n+1}}=-\phi'(0).\end{aligned}\right\} \tag{21}$$

2. Methodology

The homotopy analysis method (HAM) is an analytic approximation method for highly nonlinear problems. Thus, the resulting nonlinear system of ordinary differential equations has been investigated through homotopic technique [47, 48] for numerous values of the flow parameters. In this method auxiliary parameters are involved which offered us freedom to adjust the convergence region for velocity $(\widehat{H}'(0),\ \widehat{F}'(0),\ \widehat{G}'(0))$, temperature $\mathbf{\Theta}'(0)$ and concentration $\Phi'(0)$ profiles. The appropriate initial guesses and linear operators for the momentum, energy and concentration laws are expressed in Eqs. (22) and (23).

$$\left.\begin{aligned}&\widehat{F}_o(\Psi)=D_1\exp(-\Psi),\quad \widehat{G}_o(\Psi)=\exp(-\Psi),\\&\widehat{H}_o(\Psi)=0,\quad \Theta_o(\Psi)=\exp(-\Psi),\\&\phi_o(\Psi)=\exp(-\Psi),\end{aligned}\right\} \tag{22}$$

$$\left.\begin{aligned}&£_{\widehat{F}}=\widehat{F}''-\widehat{F},\quad £_{\widehat{G}}=\widehat{G}''-\widehat{G},\\&£_{\widehat{H}}=\widehat{H}',\quad £_\Theta=\Theta''-\Theta,\\&£_\phi=\phi''-\phi.\end{aligned}\right\} \tag{23}$$

With properties (Eq. (24))

$$\left.\begin{aligned}&£_{\widehat{F}}\left[\tilde{e}_2e^{\Psi}+\tilde{e}_3e^{-\Psi}\right]=0,\quad £_{\widehat{G}}\left[\tilde{e}_4e^{\Psi}+\tilde{e}_5e^{-\Psi}\right]=0,\\&£_{\widehat{H}}[\tilde{e}_1]=0,\quad £_\Theta\left[\tilde{e}_6e^{\Psi}+\tilde{e}_7e^{-\Psi}\right]=0,\\&£_\phi\left[\tilde{e}_8e^{\Psi}+\tilde{e}_9e^{-\Psi}\right]=0,\end{aligned}\right\} \tag{24}$$

Here, arbitrary constants are signified by $\tilde{e}_j\ with\ j=1-9$.

2.1. Analysis

One can see that permissible values for interval of convergence include $(-1.5\le h_{\widehat{F}}\le -0.2)$, $(-1.4\le h_{\widehat{H}}\le -0.5)$, $(-1.6\le h_{\widehat{G}}\le -0.4)$, $(-1.4\le h_\Theta\le -0.5)$ and $(-1.3\le h_\phi\le -0.4)$ respectively (see Fig. 2). It is noted that 20^{th}, 25^{th}, 25^{th}, 36^{th} and 30^{th} order of approximations, are sufficient for the convergence of momentum, temperature and concentration fields respectively (see Table 1). Tables 2 and 3 are studied to check the numerical estimation of Nusselt and Sherwood numbers for different emerging parameters. A comparison of present results is performed with that of Mitschka and Andersson (see Table 4). It is an obvious observation from this table that our results agree very well with their results, which confirms that code used in the present work is valid .

3. Results and discussion

The influence of sundry parameters like material parameter (B_s), Hartmann number (M_1) and the buoyancy ratio parameter (N_1), radiation parameter $(\widehat{N}_R)$, nonlinear convective parameters $(\beta_t,\ \beta_c)$, heat generation/absorption parameters $(\widehat{B}_1,\ \widehat{B}_2)$, temperature ratio factor (Θ_w), Brownian motion and thermophoresis parameters $(\widehat{N}_b, \widehat{N}_t)$, activation energy parameter $(\widehat{E}_a)$, Schmidt number (Sc), Lewis number (Le),

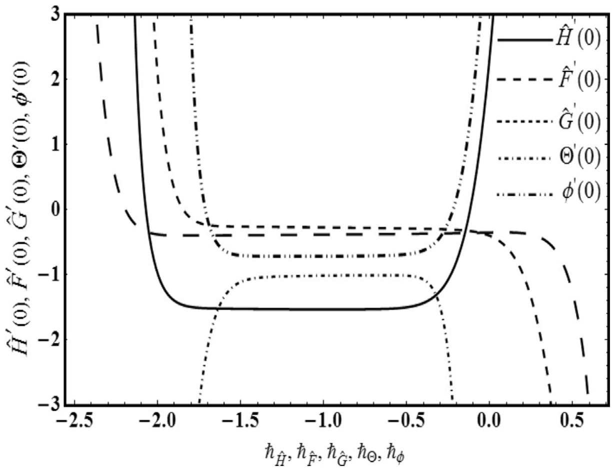

Fig. 2. h − *curves*.

Table 1

Convergence of HAM solutions when. $\tilde{\beta}_t = \tilde{\beta}_c = M_1 = \xi_2 = \widehat{N}_R = \widehat{N}_t = 0.1$, $\widehat{N}_1 = \widehat{B}_2 = D_1 = \widehat{N}_b = 0.2$, $Ec = \delta_1 = 1.0$, $Le = 0.3$, $\Pr = 1.3$ *and* $\widehat{E}_a = 0.5$.

Order of approx.	$\widehat{\mathbf{H}}'(0)$	$\widehat{\mathbf{F}}'(0)$	$\widehat{\mathbf{G}}'(0)$	$\boldsymbol{\Theta}'(0)$	$\phi'(0)$
01	−1.0138	−0.4375	−0.3165	−1.0819	−0.7398
10	−1.2344	−0.4262	−0.2964	−1.0778	−0.7374
20	−1.4362	−0.3963	−0.2801	−1.0645	−0.7360
25	−1.5360	−0.3963	−0.2855	−1.0582	−0.7357
30	−1.5360	−0.3963	−0.2885	−1.0457	−0.7352
36	−1.5360	−0.3963	−0.2885	−1.0430	−0.7352
50	−1.5360	−0.3963	−0.2885	−1.0430	−0.7352

on velocity, temperature and concentration graphs are elucidated. Figs. 3, 4, and 5 examine the influences of material parameter (B_s), stretching parameter (D_1), Hartmann number (M_1) and the buoyancy ratio parameter (N_1) on axial $\widehat{H}(\Psi)$, radial $\widehat{F}(\Psi)$ and tangential $\widehat{G}(\Psi)$ velocity distributions are observed for shear-thinning $(n < 1)$ and shear-thickening $(n > 1)$ fluids. Influence of material parameter (B_s)on radial $\widehat{F}(\Psi)$ and tangential $\widehat{G}(\Psi)$ velocity distributions are shown in Fig. 3 (a, b). Here radial $\widehat{F}(\Psi)$ and tangential $\widehat{G}(\Psi)$ velocity curves rises for greater estimation of $(B_s = 0.1, 0.5, 1.0, 1.5)$ for both shear-thinning $(n < 1)$ and shear-thickening $(n > 1)$ fluids. Higher values of (B_s) correspond to reduce fluid viscosity and fluid particles feel free to move randomly. As a result, velocity $(\widehat{F}(\Psi), \widehat{G}(\Psi))$ enhances. It is notify that velocity in shear thinning case $(n < 1)$ is more prominent than compared with shear thickening liquids $(n > 1)$ due to weaker viscosity. Salient features of Hartmann number (M_1) on radial $\widehat{F}(\Psi)$ and tangential $\widehat{G}(\Psi)$ velocity distributions is displayed in Fig. 4 (a, b) when $(n < 1)$ and $(n > 1)$. Here radial $\widehat{F}(\Psi)$ is found to be diminishing for superior values of $(M_1 = 0.2, 0.4, 0.6, 0.8)$ when $(n < 1)$ and $(n > 1)$. Physically with the rise in (M_1), Lorentz force develops extra resistance between fluid particles and thus velocity profile slows down for both shear thickening $(n > 1)$ and thinning $(n < 1)$ fluids. While opposite impact of tangential $\widehat{G}(\Psi)$ velocity is noticed against (M_1). Fig. 5 (a, b) is plotted to study the impact of velocity profiles $(\widehat{\mathrm{H}}(\Psi), \widehat{\mathrm{F}}(\Psi))$ for higher values of (D_1). Increasing trend of axial $\widehat{H}(\Psi)$ and radial $\widehat{F}(\Psi)$ velocity is noticed for higher estimation of $(D_1 = 0.2, 0.4, 0.6, 0.8)$ for both shear thickening $(n > 1)$ and thinning $(n < 1)$ fluids. This performance of velocity is because of an expansion in extending rate of plate. Figs. 6, 7, and 8 are sketched to analyze the effects of radiation parameter $(\widehat{N}_R)$, nonlinear convective parameter due to temperature (β_t), heat generation/absorption parameters $(\widehat{B}_1, \widehat{B}_2)$, temperature ratio factor (Θ_w) and Brownian motion parameter $(\widehat{N}_b)$ on $\Theta(\Psi)$ distribution respectively. Fig. 6 (a, b) defines the effect of $(\widehat{N}_R)$ and (β_t) on $\Theta(\Psi)$. Increasing tendency of $\Theta(\Psi)$ is observed for greater values of $(\widehat{N}_R = 0.2, 0.4, 0.6, 0.8)$. Since larger $(\widehat{N}_R)$ corresponds to decay in mean absorption factor that eventually upsurges the temperature $\Theta(\Psi)$ (see Fig. 6 (a)). Temperature $\Theta(\Psi)$ is found to be increasing function of nonlinear convection parameter (β_t) (see Fig. 6 (b)). Since motion of

Table 2

Numerical values of $Nu_z(Re_{\beta_1})^{-\frac{1}{(n+1)}}$ when $\tilde{\beta}_t = \tilde{\beta}_c = M_1 = 0.1, \widehat{N}_1 = \widehat{B}_2 = D_1 = 0.2$, $Ec = \delta_1 = 1.0$, $Le = 0.3$ and $\widehat{E}_a = 0.5$.

Bs		Pr	$\widehat{N}_R$	ξ_2	$\widehat{N}_t$	$Nu_z(Re_{\beta_1})^{-\frac{1}{(n+1)}}$	
						n = 0.6	n = 1.8
0.5	0.2	1.2	0.6	0.3	0.3	1.9245	2.0124
1.0						1.9819	2.0959
1.5						2.0485	2.1905
	0.2					1.9245	2.0124
	0.4					1.8931	1.9728
	0.6					1.8362	1.9423
		7.2				1.8733	1.9478
		1.2				1.9245	2.0124
		2.5				2.0318	2.1247
			0.2			1.7991	1.8645
			0.4			1.8847	1.9638
			0.6			1.9245	2.0124
				0.1		1.9247	2.0127
				0.3		1.9245	2.0124
				0.5		1.9241	2.0120
					0.3	1.9245	2.0124
					0.5	1.8905	1.9767
					0.7	1.8147	1.9054

Table 3

Numerical values of $\mathrm{Sh}_z(\mathrm{Re}_{\beta_1})^{-\frac{1}{(n+1)}}$ when $\tilde{\beta}_t = \tilde{\beta}_c = M_1 = 0.1$, $\widehat{N}_1 = \widehat{B}_2 = D_1 = 0.2$, $Ec = \delta_1 = 1.0$, $Le = 0.3$ and $\widehat{E}_a = 0.5$.

Bs		Pr	$\widehat{N}_R$	ξ_2	$\widehat{N}_t$	$\mathbf{Sh_z}(\mathbf{Re}_{\beta_1})^{-\frac{1}{(n+1)}}$	
						n = 0.6	n = 1.8
0.5	0.2	1.2	0.6	0.3	0.3	1.9179	2.0480
1.0						1.9448	2.0811
1.5						1.9760	2.1217
	0.2					1.9179	2.0480
	0.4					1.9565	2.0926
	0.6					1.9957	2.1743
		7.2				1.9578	2.0915
		1.2				1.9179	2.0480
		2.5				1.8653	2.0075
			0.2			1.8466	2.0098
			0.4			1.8834	2.0161
			0.6			1.9179	2.0480
				0.1		1.8904	2.0217
				0.3		1.9179	2.0480
				0.5		1.9450	2.0740
					0.3	1.9179	2.0480
					0.5	1.8834	2.0276
					0.7	1.8802	2.0061

Table 4

Comparison of $\widehat{\mathrm{F}}'(0)$ and $\widehat{\mathrm{G}}'(0)$ with [49] and [50] when $\beta_t = \beta_c = B_s = D_1 = M_1 = N_1 = 0$.

n	$\widehat{\mathbf{F}}'(0)$			$\widehat{\mathbf{G}}'(0)$		
	Present (HAM)	Ref. [49]	Ref. [50]	Present (HAM)	Ref. [49]	Ref. [50]
0.6	0.500	0.500	0.501	0.677	0.677	0.676
0.8	0.504	0.504	0.504	0.635	0.636	0.636
1.0	0.511	0.510	0.510	0.616	0.616	0.616
1.8	0.529	0.529	0.529	0.601	0.601	0.601

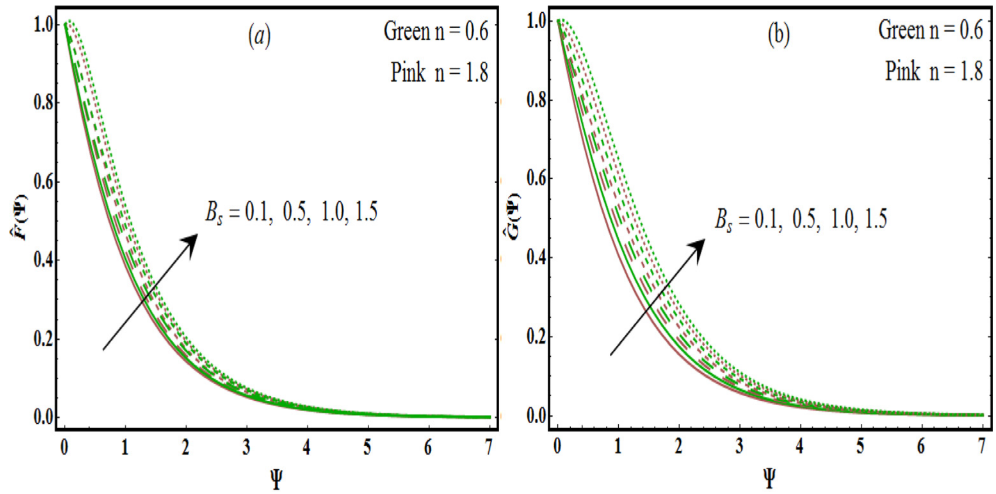

Fig. 3. $\widehat{\mathrm{F}}(\Psi)$ and $\widehat{\mathrm{G}}(\Psi)$ against $\mathrm{B_s}$.

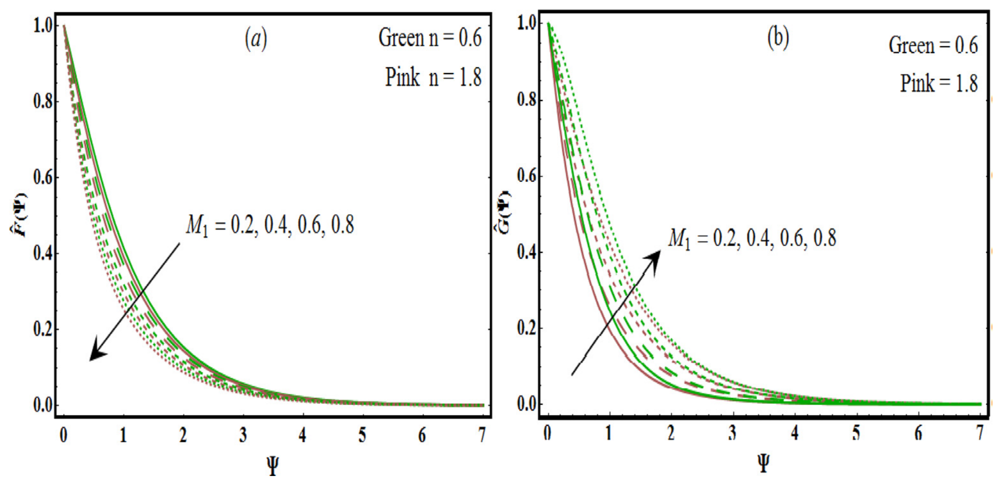

Fig. 4. $\widehat{\mathrm{F}}(\Psi)$ and $\widehat{\mathrm{G}}(\Psi)$ against M_1.

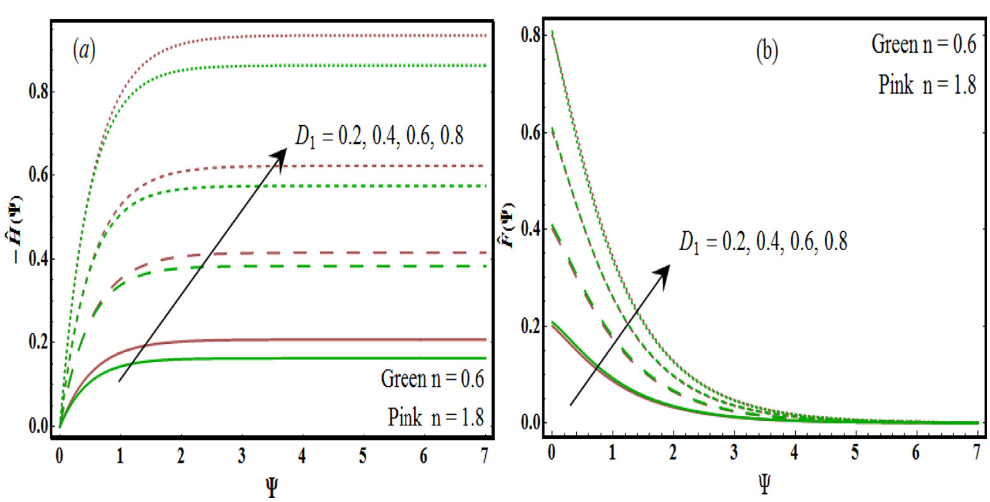

Fig. 5. $\widehat{\mathrm{H}}(\Psi)$and $\widehat{\mathrm{F}}(\Psi)$ against D_1.

fluid particles increases for higher approximation of $(\beta_t = 0.2, 0.4, 0.6, 0.8)$ for shear thinning $(n < 1)$ and shear thickening $(n > 1)$ fluids. In fact, for higher (β_t), temperature difference $(T_w - T_\infty)$ enhances which is accountable for velocity augmentation and ultimately temperature $\Theta(\Psi)$ rises. Fig. 7 (a, b) is schemed to study the characteristics of $\Theta(\Psi)$ for greater non-uniform heat source/sink parameters $(\widehat{B}_1, \widehat{B}_2)$ respectively. Technically, increasing values of $(\widehat{B}_1 = 0.2, 0.4, 0.6, 0.8)$ and $(\widehat{B}_2 = 0.1,$

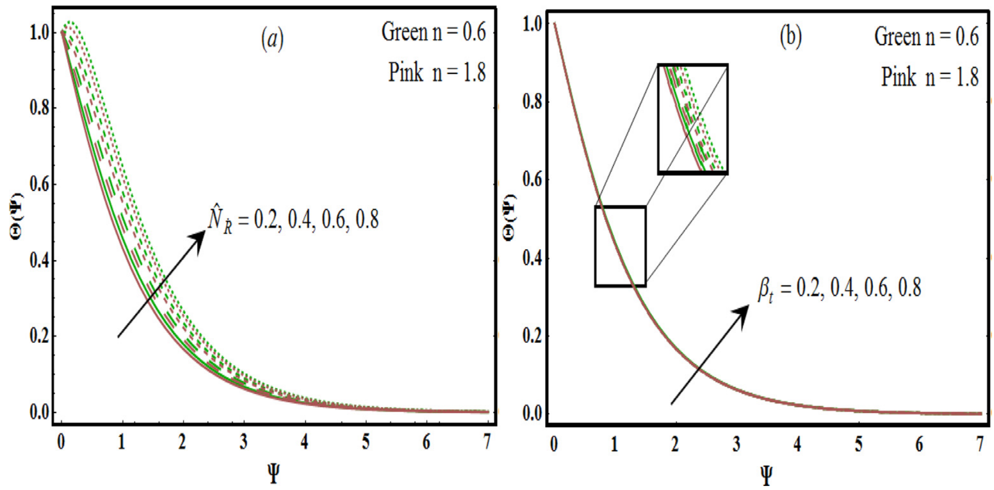

Fig. 6. $\Theta(\Psi)$ against $\widehat{N}_R$ and β_t.

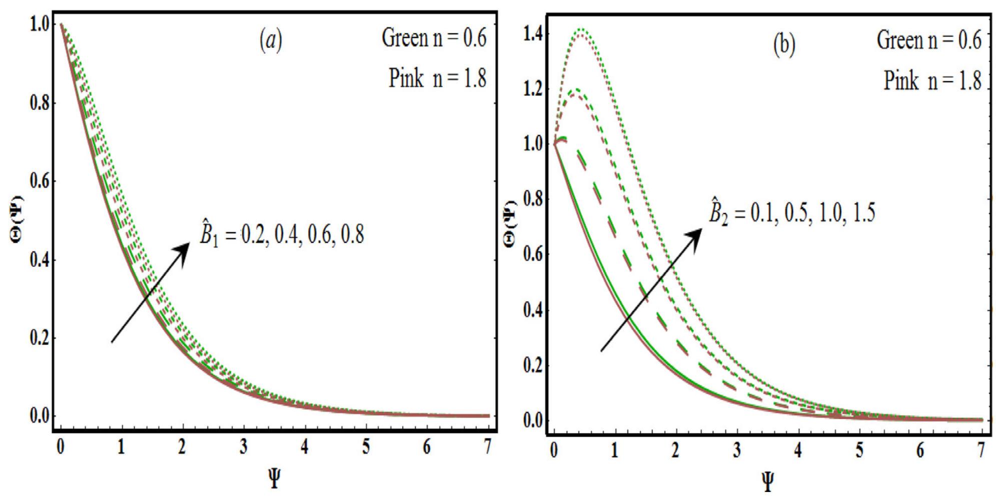

Fig. 7. $\Theta(\Psi)$ against $\widehat{B}_1$ and $\widehat{B}_2$.

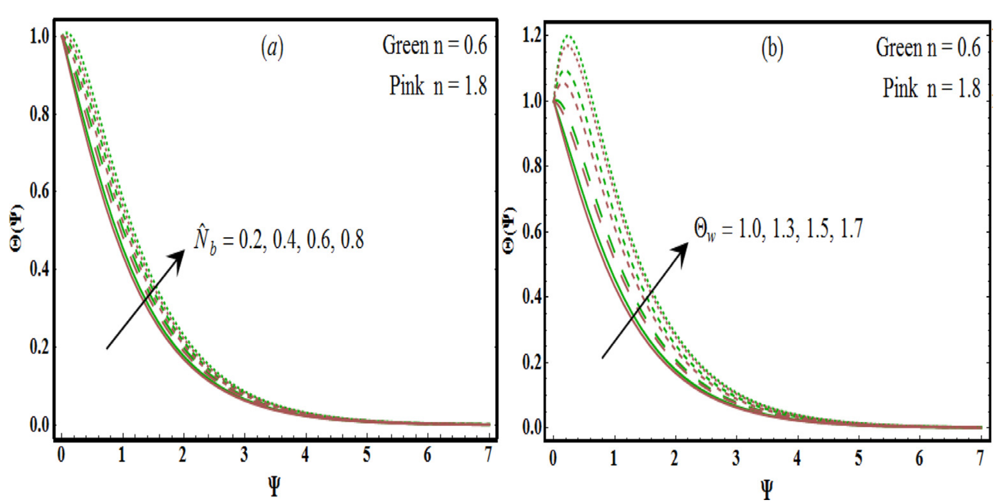

Fig. 8. $\Theta(\Psi)$ against $\widehat{N}_b$ and Θ_w.

$0.5, 1.0, 1.5)$ performs as an agent to produce more heat. Since positive values of $(\widehat{B}_1)$ and $(\widehat{B}_2)$ acts like heat generators and negative values is for heat absorbers. Normally, increase in heat source becomes a source of enrichment in the thermal boundary thickness. Fig. 8 (a, b) shows the behavior of $(\widehat{N}_b = 0.2, 0.4, 0.6, 0.8)$ and $(\Theta_w = 1.0, 1.3, 1.5, 1.7)$ on temperature $\Theta(\Psi)$ curve. Here $\Theta(\Psi)$ is found to be upsurge in view

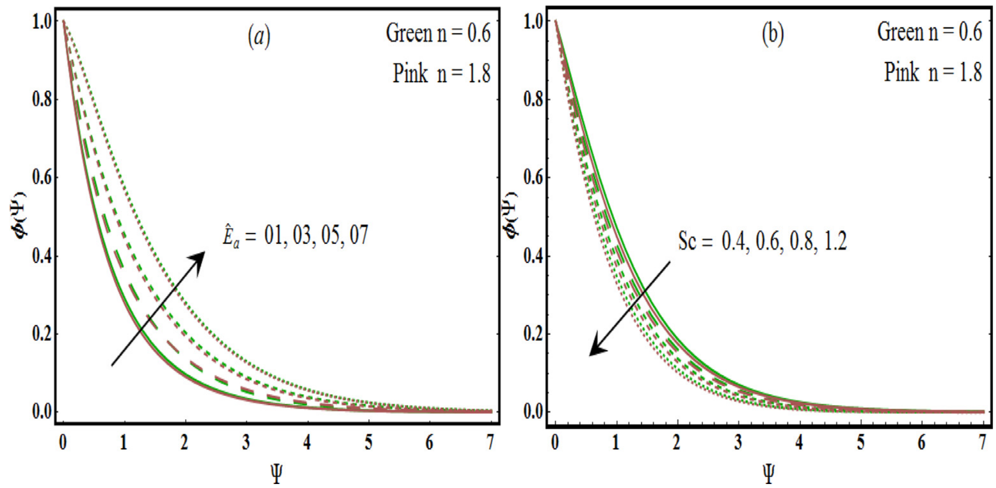

Fig. 9. $\phi(\Psi)$ against $\widehat{E}_a$ and Sc.

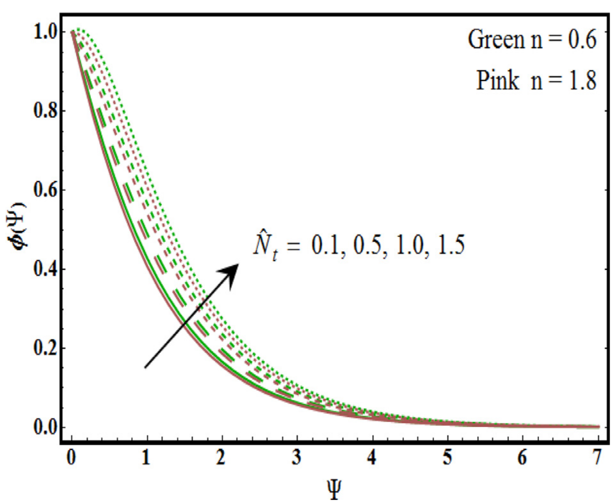

Fig. 10. $\phi(\Psi)$ against $\widehat{N}_t$.

of $(\widehat{N}_b)$. In fact, more heat is generated through the random collision of fluid particles within the frame of larger $(\widehat{N}_b)$. Therefore $\Theta(\Psi)$ increases for both $n < 1$ *and* $n > 1$ cases. Equivalent enhancing trend of $\Theta(\Psi)$ for shear-thinning $(n < 1)$ and shear-thickening $(n > 1)$ fluids against (Θ_w) can be viewed in Fig. 8 (b). For higher pattern of $(\Theta_w = 1.0, 1.3, 1.5, 1.7)$ liquid temperature is considerably more than the ambient temperature (T_∞) which upsurges thermal condition of the liquid. Fig. 9 (a, b) study the influence of activation energy (E_a) and Schmidt number (Sc) on concentration $\phi(\Psi)$ profile. In fact, greater $(E_a = 1.0, 3.0, 5.0, 7.0)$ diminishes the modified Arrhenius function that endorses the generative chemical reaction in the end. Hence $\phi(\Psi)$ enriches. The concentration $\phi(\Psi)$ and solutal boundary layer thickness declines for larger Sc (see Fig. 9 (b)). According to the definition, Schmidt number is ratio of momentum to mass diffusivities. Thus for larger $(Sc = 0.4, 0.6, 0.8, 1.2)$ the mass diffusivity decreases which is responsible in reduction of concentration $\phi(\Psi)$. Fig. 10 exhibits that both concentration $\phi(\Psi)$ and boundary layer thickness are heightened for greater values of $(\widehat{N}_t = 0.1, 0.5, 1.0, 1.5)$. The thermal conductivity of the fluid enriches in presence of nanoparticles. Therefore, higher $(\widehat{N}_t)$ exaggerate heat conductivity of the fluid. Such greater thermal conductivity becomes a source of rise in $\phi(\Psi)$. Figs.11, 12, 13, 14, 15, and 16 are constructed to analyze the entropy number $(\widehat{N}_G)$ and Bejan number $(\widehat{Be})$ for greater values of involved parameters like material parameter (B_s), Hartmann number (M_1), Brinkman number $(\widehat{Br})$, reaction rate factor (ξ_3), diffusion parameter (L^*) and radiation parameter $(\widehat{N}_R)$ respectively. Consequence of (B_s) on $(\widehat{N}_G)$ and $(\widehat{Be})$ is sketched in Fig 11 (a, b). Greater estimation of (B_s) lessen entropy generation $(\widehat{N}_G)$ and reverse effect is detected for Bejan number $(\widehat{Be})$. Since higher values of $(B_s = 0.1, 0.3, 0.5, 0.7)$ leads to an increase in shear rate of viscosity which decelerates the fluid motion. As a result $(\widehat{N}_G)$ diminishes for both $n < 1$ and $n > 1$ cases. Declining role of $(\widehat{Be})$ is

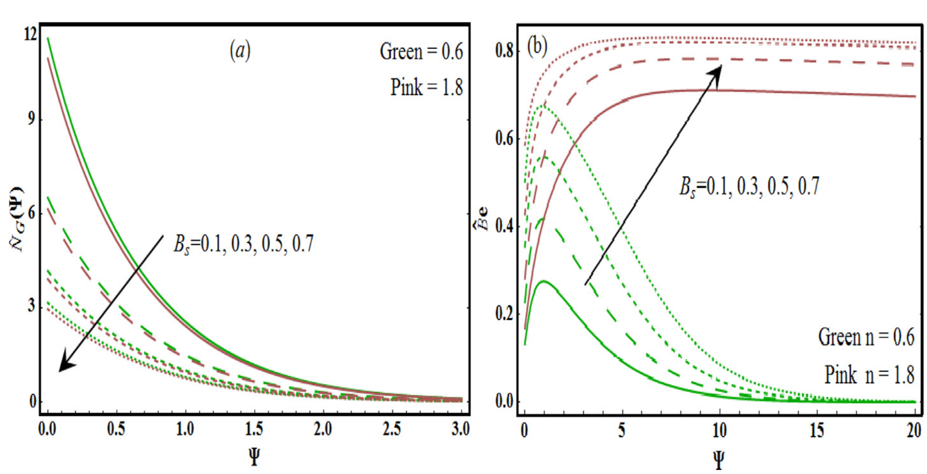

Fig. 11. $\widehat{N}_G(\Psi)$ and $\widehat{Be}(\Psi)$ against B_s.

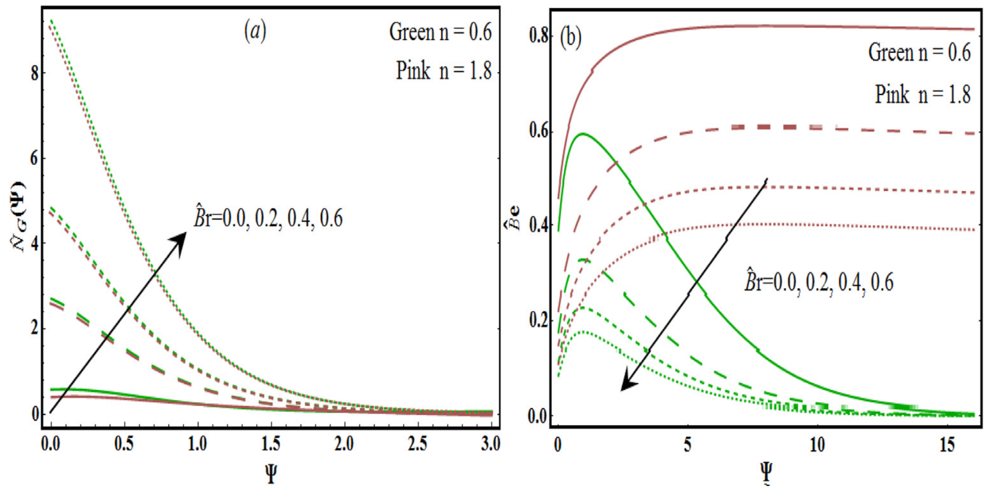

Fig. 12. $\widehat{N}_G(\Psi)$ and $\widehat{Be}(\Psi)$ against $\widehat{Br}$. .

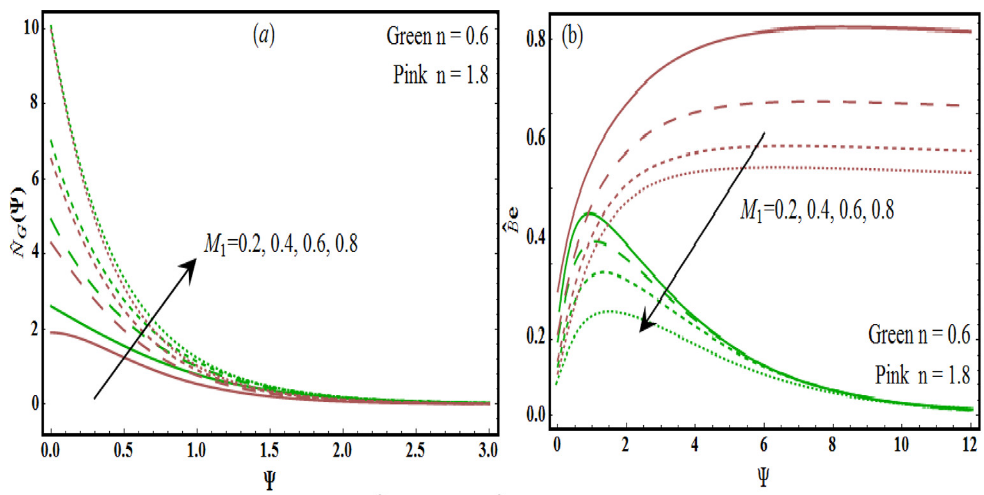

Fig. 13. $\widehat{N}_G(\Psi)$ and $\widehat{Be}(\Psi)$ against M_1.

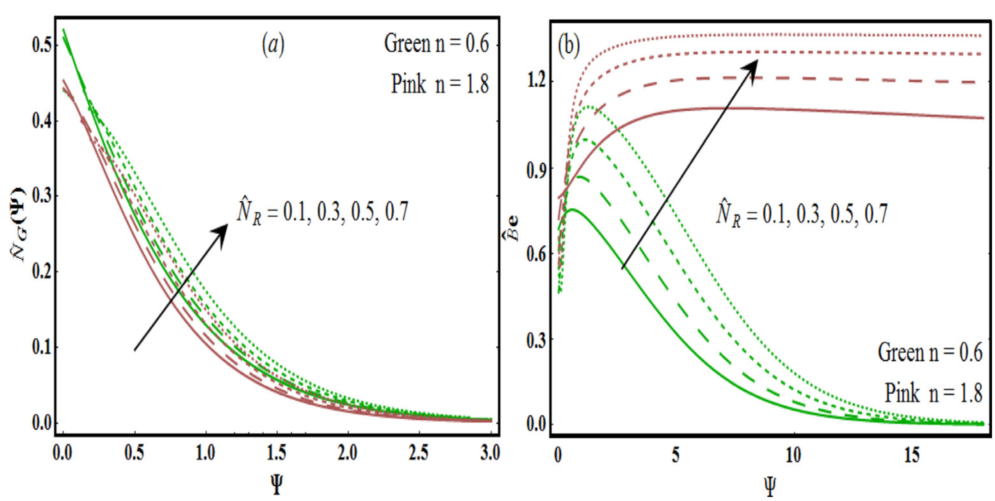

Fig. 14. $\widehat{N}_G(\Psi)$ and $\widehat{Be}(\Psi)$ against $\widehat{N}_R$.

inspected for greater values of $(B_s = 0.1, 0.3, 0.5, 0.7)$ because heat transfers dominant over the viscous effects (see Fig. 11 (b)). Variation of $(\widehat{N}_G)$ and $(\widehat{Be})$ for enhancing Brinkman number $(\widehat{Br})$ is displayed in Fig. 12 (a, b). It is remarked that $(\widehat{N}_G)$ increases for growing values of (Br) while reverse nature is identified for Bejan number $(\widehat{Be})$. There exists massive quantity of heat in the system with an increase in $(\widehat{Br} = 0.0, 0.2,$

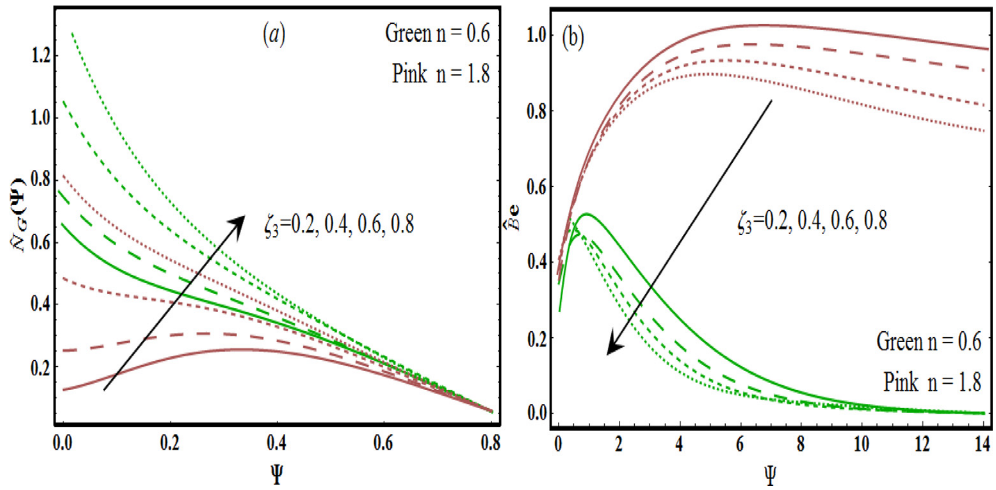

Fig. 15. $\widehat{N}_G(\Psi)$ and $\widehat{B}e(\Psi)$ against ξ_3.

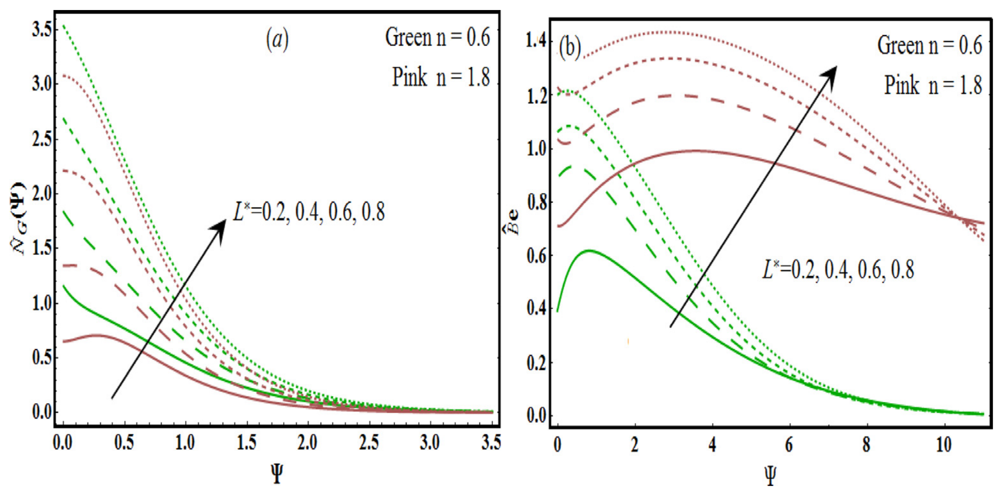

Fig. 16. $\widehat{N}_G(\Psi)$ and $\widehat{B}e(\Psi)$ against L^*.

0.4, 0.6). In fact, $(\widehat{B}r)$ is heat transfer by molecular conduction in comparison of heat production by viscous heating, which is responsible for rise in disorderedness of the system. Additionally, $(\widehat{B}e)$ is diminished for higher $(\widehat{B}r = 0.0, 0.2, 0.4, 0.6)$ due to dominant role of viscous effects over heat transfer effects. Feature of (M_1) on entropy generation $(\widehat{N}_G)$ and Bejan number $(\widehat{B}e)$ is exhibited in Fig. 13 (a, b). Enhancing character of $(\widehat{N}_G)$ is pragmatic while opposite influence of $(\widehat{B}e)$ is remarked. For greater $(M_1 = 0.2, 0.4, 0.6, 0.8)$, more resistance is developed that causes $(\widehat{N}_G)$ to be enhanced (see Fig. 13 (a)). In the present situation, viscous effects dominant over heat and mass transfer effects for greater estimation of $(M_1 = 0.2, 0.4, 0.6, 0.8)$. Hence $(\widehat{B}e)$ diminishes. Fig. 14 (a, b) is sketched to explore the nature of radiation parameter $(\widehat{N}_R)$ on $(\widehat{N}_G)$ and $(\widehat{B}e)$. Here, entropy generation (irreversibility) and Bejan number are intensifying for greater values of $(\widehat{N}_R = 0.1, 0.3, 0.5, 0.7)$. Since, there exists a direct relationship between internal energy $(\widehat{B}e)$ and entropy generation $(\widehat{N}_G)$ with $(\widehat{N}_R)$. Fig. 15 (a, b) reveals that reverse behavior of $(\widehat{N}_G)$ and $(\widehat{B}e)$ is identified for larger values of $(\xi_3 = 0.2, 0.4, 0.6, 0.8)$. Since chemical reaction rate $(\widehat{K}_R^2)$ gradually enriches for larger estimation of (ξ_3), that is accountable for an upsurge in $(\widehat{N}_G)$. Fig. 16 (a, b) indicates the impact of $(\widehat{N}_G)$ and $(\widehat{B}e)$ for fixed values of diffusion parameter (L^*). Similar enhancing behavior of both $(\widehat{N}_G)$ and $(\widehat{B}e)$ is

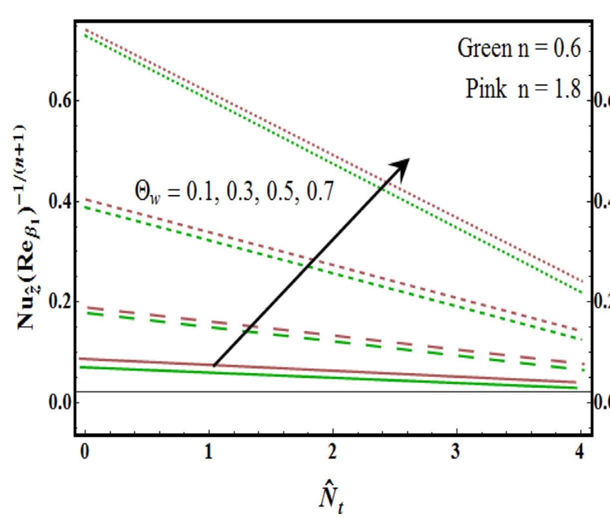

Fig. 17. $\mathrm{Nu}_{\hat{z}}(\mathrm{Re}_{\beta_1})^{-\frac{1}{n+1}}$ with Θ_w.

noticed for higher values of $(L^* = 0.2, 0.4, 0.6, 0.8)$. Since diffusivity in the fluid particle increases that directly corresponds to produce more disorderness and ultimately, entropy generation upsurges (see Fig. 16 (a)). It

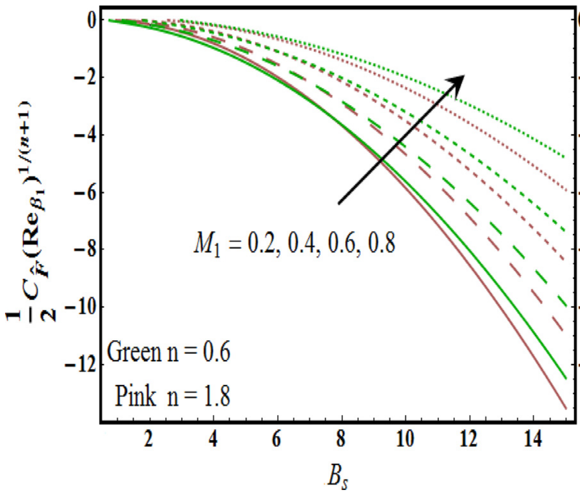

Fig. 18. $\frac{1}{2}C_{\widehat{F}}(Re_{\beta_1})^{1/(n+1)}$ with M_1.

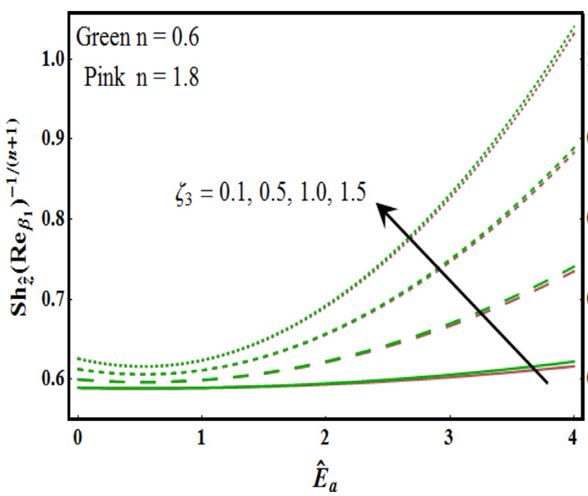

Fig. 19. $Sh_{\widehat{z}}(Re_{\beta_1})^{-\frac{1}{n+1}}$ with ξ_3.

is found from Fig. 16 (b) that an increase in (L^*) leads to rise in the Bejan number $(\widehat{B}e)$. It is due to the fact that, for higher $(L^* = 0.2, 0.4, 0.6, 0.8)$ heat and mass transfer preeminent over viscous effects. From Figs. 11, 12, 13, 14, 15, and 16, it is perceived that entropy generation $(\widehat{N}_G)$ is always prominent for shear thinning fluid $n < 1$ while $(\widehat{B}e)$ has larger impact for shear thickening liquids $n > 1$. Local Nusselt number $\left(Nu_{\widehat{z}}(Re_{\beta_1})^{-\frac{1}{n+1}}\right)$, skin friction coefficient $\left(\frac{1}{2}C_{\widehat{F}}(Re_{\beta_1})^{1/(n+1)}\right)$ and Sherwood number $\left(Sh_{\widehat{z}}(Re_{\beta_1})^{-\frac{1}{n+1}}\right)$ are presented in Figs. 17, 18, and 19 for emerging parameters (Θ_w), $(\widehat{N}_t)$, (M_1), (B_s), (E_a), and (ξ_3). Variation of heat transfer rate with (Θ_w) and $(\widehat{N}_t)$ are discussed through Fig. 17. It is ascertained that Nusselt number is heightened for both $(\Theta_w = 0.1, 0.3, 0.5, 0.7)$ and $(\widehat{N}_t)$. Fig. 18 revealed that skin friction coefficent is an increasing function of (B_s) and $(M_1 = 0.2, 0.4, 0.6, 0.8)$. For larger (E_a) and $(\xi_3 = 0.1, 0.5, 1.0, 1.5)$, enhancing character of Sherwood number is observed for both shear thinning $n < 1$ and shear thickening $n > 1$ fluids (see Fig. 19).

4. Conclusion

Present study carried out speculative investigation of entropy generation optimization and activation energy for convective flow of Sisko nanofluid over a stretchable rotating disk. In addition, combined effects of Joule heating, nonlinear mixed convection, non-uniform heat generation/absorption and viscous dissipation are also factored into the analysis. The series solution of the governing set of differential equations is accomplished by employing Homotopy method. The presented analysis has the following observations:

- ≻ Temperature $\boldsymbol{\Theta}(\boldsymbol{\Psi})$ rises for greater estimation of Brownian motion parameter $(\widehat{N}_b)$, nonlinear thermal mixed convection parameter (β_t), radiation parameter $(\widehat{\mathbf{N}}_\mathbf{R})$ **and** temperature ratio factor $(\boldsymbol{\Theta}_w)$.
- ≻ Remarkable behavior of temperature $\boldsymbol{\Theta}(\boldsymbol{\Psi})$ is noticed for pseudo-plastic fluids $(n < 1)$.
- ≻ Concentration $\phi(\boldsymbol{\Psi})$ curve reduces for higher values of (Sc) while reverse impact is observed for both $(\widehat{N}_t)$ and (E_a).
- ≻ Magnitude of axial $\widehat{\mathbf{H}}(\boldsymbol{\Psi})$, radial $\widehat{\mathbf{F}}(\boldsymbol{\Psi})$ and tangential $\widehat{\mathbf{G}}(\boldsymbol{\Psi})$ velocity profiles enhances for greater estimation of material parameter $(\mathbf{B}_s)$.
- ≻ Entropy generation $(\widehat{N}_G)$ enhances for higher estimation of parameters $(\widehat{B}r)$, (ξ_3), $(\mathbf{M}_1)$, $(\mathbf{L}^*)$ **and** $(\widehat{\mathbf{N}}_\mathbf{R})$, while it decays for (B_s).
- ≻ Entropy generation is more for shear thinning fluids $(n < 1)$ whereas Bejan number $(\widehat{B}e)$ is prominent for shear thickening fluids $(n > 1)$.
- ≻ Bejan number $(\widehat{B}e)$ is greater for $(\widehat{N}_R)$ ***and*** (B_s) while it declines for (ξ_3), $(\mathbf{M}_1)$ **and** $(\widehat{\mathbf{B}}\mathbf{r})$.

Declarations

Author contribution statement

Misbah Ijaz: Performed the experiments; Analyzed and interpreted the data; Wrote the paper.

Muhammad Ayub, Hammad Khan: Conceived and designed the experiments; Performed the experiments.

Funding statement

This research did not receive any specific grant from funding agencies in the public, commercial, or not-for-profit sectors.

Competing interest statement

The authors declare no conflict of interest.

Additional information

No additional information is available for this paper.

References

[1] Z. Hu, W. Lu, M.D. Thouless, Slip and wear at a corner with Coulomb friction and an interfacial strength, Wear 338 (2015) 242–251.
[2] Z. Hu, W. Lu, M.D. Thouless, J.R. Baber, Effect of plastic deformation on the evolution of wear and local stress fields in fretting, Int. J. Solids Struct. 82 (2016) 1–8.
[3] H. Wang, Z. Hu, W. Lu, M.D. Thouless, The effect of coupled wear and creep during grid-to-rod fretting, Nucl. Eng. Des. 318 (2017) 163–173.
[4] T. Von Karman, Uber laminare und turbulente Reibung, Z. Angew. Math. Mech. 1 (1921) 233–252.
[5] M. Turkyilmazoglu, MHD fluid flow and heat transfer due to a stretching rotating disk, Int. J. Therm. Sci. 51 (2012) 195–201.
[6] M. Khan, T. Salahuddin, M.Y. Malik, Impact of enhancing diffusion on Carreau–Yasuda fluid flow over a rotating disk with slip conditions, J. Braz. Soc. Mech. Sci. Eng. 41 (2019) 78.
[7] O.D. Makinde, A.S. Eegunjobi, M.S. Tshehla, Thermodynamics analysis of variable viscosity hydromagnetic Couette flow in a rotating system with Hall effects, Entropy 17 (2015) 7811–7826.
[8] T. Hayat, S. Qayyum, M. Imtiaz, A. Alsaedi, Radiative flow due to a stretchable rotating disk with variable thickness, Results Phys. 7 (2017) 156–165.
[9] M.J. Babu, N. Sandeep, Three-dimensional MHD slip flow of nanofluids over a slandering stretching sheet with thermophoresis and Brownian motion effects, Adv. Powder Technol. 27 (2016) 2039–2050.

[10] T. Hayat, M. Imtiaz, A. Alsaedi, S. Asghar, Slip flow by a variable thickness rotating disk subject to magneto-hydrodynamics, Results Phys. 7 (2017) 503–509.
[11] M.M. Rashidi, S. Abelman, N.F. Mehr, Entropy generation in steady MHD flow due to a rotating porous disk in a nanofluid, Int. J. Heat Mass Transf. 62 (2013) 515–525.
[12] T. Hayat, M. Rashid, M. Imtiaz, A. Alsaedi, Magneto-hydrodynamic (MHD) flow of Cu water nanofluid due to a rotating disk with partial slip, AIP Adv. 5 (2015), 067169.
[13] T. Hayat, S. Qayyum, S.A. Shehzad, A. Alsaedi, Simultaneous effects of heat generation/absorption and thermal radiation in magneto-hydrodynamics (MHD) flow of Maxwell nanofluid towards a stretched surface, Results Phys. 7 (2017) 562–573.
[14] C.S.K. Raju, N. Sandeep, A. Malvandi, Free convective heat transfer of MHD Cu-kerosene nanofluid over a cone with temperature dependent viscosity, Acta Astronaut. 129 (2016) 419–428.
[15] E. Magyari, A. Pantokratoras, Note on the effect of thermal radiation in the linearized Rosseland approximation on the heat transfer characteristics of various boundary layer flows, Int. Commun. Heat Mass Transf. 38 (2011) 554–556.
[16] A. Pantokratoras, Natural convection along a vertical isothermal plate with linear and nonlinear Rosseland thermal radiation, Int. J. Therm. Sci. 84 (2014) 151–157.
[17] M. Khan, T. Salahuddin, A. Tanveer, M.Y. Malik, A. Hussain, Change in internal energy of thermal diffusion stagnation point Maxwell nanofluid flow along with solar radiation and thermal conductivity, Chin. J. Chem. Eng. (2019).
[18] A. Mushtaq, M. Mustafa, T. Hayat, A. Alsaedi, On the numerical solution of the nonlinear radiation heat transfer problem in a three-dimensional flow, Z. Naturforsch. 69 (2014) 705–713.
[19] M. Ijaz, M. Ayub, Simulation of magnetic dipole and dual stratification in radiative flow of ferromagnetic Maxwell fluid, Heliyon 5 (2019), e01465.
[20] S.K. Parida, S. Panda, B.R. Rout, MHD boundary layer slip flow and radiative nonlinear heat transfer over a flat plate with variable fluid properties and thermophoresis, Alexandria Eng. J. 54 (2015) 941–953.
[21] R. Cortell, Fluid flow and radiative nonlinear heat transfer over a stretching sheet, J. King Saud Univ. Sci. 26 (2014) 161–167.
[22] M.I. Afridi, M. Qasim, O.D. Makinde, Second law analysis of boundary layer flow with variable fluid properties, J. Heat Transf. 139 (10) (2017) 104505.
[23] S.A. Shehzad, T. Hayat, A. Alsaedi, M.A. Obid, Nonlinear thermal radiation in three-dimensional flow of Jeffrey nanofluid: a model for solar energy, Appl. Math. Comput. 248 (2014) 273–286.
[24] O.D. Makinde, F. Mabood, S.M. Ibrahim, Chemically reacting on MHD boundary layer flow of nanofluids over a nonlinear stretching sheet with heat source/sink and thermal radiation, Therm. Sci. 22 (1B) (2018) 495–506.
[25] O.D. Makinde, T. Iskander, F. Mabood, M.S. Tshehla, MHD Couette-Poiseuille flow of variable viscosity nanofluids in a rotating permeable channel with Hall effects, J. Mol. Liq. 221 (2016) 778–787.
[26] A.W. Sisko, The flow of lubricating greases, Ind. Eng. Chem. Res. 50 (1958) 1789–1792.
[27] T. Hayat, R.J. Moitsheki, S. Abelman, Stokes' first problem for Sisko fluid over a porous wall, Appl. Math. Comput. 217 (-) (2010) 622–628.
[28] R. Malik, M. Khan, A. Munir, W.A. Khan, Flow and heat transfer in Sisko fluid with convective boundary condition, PLoS One 10 (2014), e107989.
[29] A. Munir, A. Shahzad, M. Khan, Convective flow of Sisko fluid over a bidirectional stretching surface, PLoS One 10 (2015), e0130342.
[30] M. Khan, R. Malik, Forced convective heat transfer to Sisko nanofluid past a stretching cylinder in the presence of variable thermal conductivity, J. Mol. Liq. 218 (2016) 1–7.
[31] T. Hayat, M. Ijaz, S. Qayyum, M. Ayub, A. Alsaedi, Mixed convective stagnation point flow of nanofluid with Darcy-Fochheimer relation and partial slip, Results Phys. 9 (2018) 771–778.
[32] M. Sheikholeslami, R. Ellahi, H.R. Ashorynejad, G. Domairry, T. Hayat, Effects of heat transfer in flow of nanofluids over a permeable stretching wall in a porous medium, J. Comput. Theor. Nanosci. 11 (2014) 486–496.
[33] M. Sheikholeslami, D.D. Ganji, Magneto-hydrodynamic flow in a permeable channel filled with nanofluid, Sci. Iran. 21 (2014) 203–212.
[34] S. Abbasbandy, M. Yurusoy, H. Gulluce, Analytical solutions of nonlinear equations of power-law fluids of second grade over an infinite porous plate, Math. Comput. Appl. 19 (2014) 124–133.
[35] M. Bibi, M.Y. Malik, A. Zeeshan, Numerical analysis of unsteady magneto-biphase Williamson fluid flow with time dependent magnetic field, Commun. Theor. Phys. 71 (2019) 143–151.
[36] Y. Lin, L. Zheng, G. Chen, Unsteady flow and heat transfer of pseudoplastic nanoliquid in a finite thin film on a stretching surface with variable thermal conductivity and viscous dissipation, Powder Technol. 274 (2015) 324–332.
[37] M. Zubair, M. Ijaz, T. Abbas, A. Riaz, Analysis of modified Fourier law in flow of ferromagnetic Powell-Eyring fluid considering two equal magnetic dipoles, Can. J. Phys. (2018).
[38] T. Hayat, S. Qayyum, M. Imtiaz, A. Alsaedi, Three-dimensional rotating flow of Jeffrey fluid for Cattaneo-Christov heat flux model, AIP Adv. 6 (2016), 025012.
[39] T. Hayat, M. Imtiaz, A. Alsaedi, M.A. Kutbi, MHD three-dimensional flow of nanofluid with velocity slip and nonlinear thermal radiation, J. Magn. Magn. Mater. 39 (2015) 31–37.
[40] M. Khan, A. Shahzad, On boundary layer flow of a Sisko fluid over a stretching sheet, Quaest. Math. 36 (2013) 137–151.
[41] M. Ijaz, M. Ayub, M. Zubair, A. Riaz, On stratified flow of ferromagnetic nanofluid with heat generation/absorption, Phys. Scripta (2018).
[42] A. Noghrehabadi, M.R. Saffarian, R. Pourrajab, M. Ghalambaz, Entropy analysis for nanofluid flow over a stretching sheet in the presence of heat generation/absorption and partial slip, J. Mech. Sci. Technol. 27 (2013) 927–937.
[43] S. Nadeem, M.Y. Malik, N. Abbas, Heat transfer of three dimensional micropolar fluids on Riga plate, Can. J. Phys. (2019).
[44] S. Das, S. Chakraborty, R.N. Jana, O.D. Makinde, Entropy analysis of unsteady magneto-nanofluid flow past accelerating stretching sheet with convective boundary condition, Appl. Math. Mech. 36 (12) (2015) 1593–1610.
[45] S. Das, S. Chakraborty, O.D. Makinde, R.N. Jana, Entropy analysis of MHD variable thermal conductivity fluid flow past a convectively heated stretching cylinder, Defect Diffusion Forum 387 (2018) 244–259.
[46] T. Hayat, M.I. Khan, S. Qayyum, A. Alsaedi, M.I. Khan, New thermodynamics of entropy generation minimization with nonlinear thermal radiation and nano-materials, Phys. Lett. 382 (2018) 749–760.
[47] P.D. Ariel, Generalized three-dimensional flow due to a stretching sheet, Z. Angew. Math. Mech. 83 (2003) 844–852.
[48] A. Shahzad, M. Khan, A. Munir, Convective heat transfer to Sisko fluid over a nonlinear radially stretching sheet, Heat Transf. Studies Appl. 13 (2015) 341–363.
[49] P. Mitschka, J. Ulbrecht, Nicht-Newtonsche Flüssigkeiten IV. Strömung Nicht-Newtonscher Flüssigkeiten Ostwald-de Waeleschen Typs in der Umgebung Rotierender Drehkegel und Schieben, Collect. Czechoslov. Chem. Commun. 30 (1965) 2511–2526.
[50] H.I. Andersson, E. de Korte, R. Meland, Flow of a power-law fluid over a rotating disk revisited, Fluid Dyn. Res. 28 (2001) 75–88.